

**FEDSM2009-78167**

## ANALYTICAL SOLUTIONS FOR LAMINAR FULLY-DEVELOPED FLOW IN MICROCHANNELS WITH NON-CIRCULAR CROSS-SECTION

**A. Tamayol**  
PhD Student  
ata42@sfu.ca

**M. Bahrami**  
Assistant Professor  
mbahrami@sfu.ca

**Mechatronic Systems Engineering,  
School of Engineering Science,  
Simon Fraser University, BC, Canada**

### ABSTRACT

Analytical solutions are presented for laminar fully-developed flow in micro/minichannels of hyperelliptical and regular polygonal cross-sections. The considered geometries cover a wide range of common simply connected shapes including circle, ellipse, rectangle, rhomboid, star-shape, equilateral triangle, square, pentagon, and hexagon. Therefore, the present approach can be considered as a general solution. Predicted results for the velocity distribution and pressure drop are successfully compared with existing analytical solutions and experimental data collected from various sources for a variety of geometries, including: polygonal, rectangular, circular, elliptical, and rhombic cross-sections.

### NOMENCLATURE

$a$	=	Hyperellipse major axis, $m$
$A$	=	Cross-sectional area, $m^2$
$b$	=	Hyperellipse minor axis, $m$
$D_h$	=	Hydraulic diameter, $4A/\Gamma_c$ , $m$
$f$	=	Fanning friction factor
$fRe$	=	Poiseuille number
$I_p$	=	Polar moment of inertia about the centroid, $m^4$
$m$	=	Number of sides in regular polygonal ducts
$n$	=	Exponent in hyperellipse formula
$P$	=	Pressure, $N/m^2$
$Q$	=	Volumetric flow rate, $m^3/s$
$Re$	=	Reynolds number
$s$	=	Half the length of the sides in polygonal ducts, $m$
$u$	=	Axial velocity, $m/s$
$u^*$	=	Non-dimensional velocity, Eq. (7)

*Greek symbols*

$\Gamma(.)$	=	Gama function
$\Gamma_c$	=	Perimeter, $m$
$\varepsilon$	=	Cross-sectional aspect ratio, $\varepsilon = b/a$
$\eta$	=	Non-dimensional coordinate, $\eta = r/a$
$\mu$	=	Viscosity, $N \cdot s/m^2$
<i>Subscript</i>		
$\sqrt{A}$	=	Square root of cross-sectional area, $m$

### 1 INTRODUCTION

The fast growth of microfluidic systems and their applications in microelectronic cooling [1], MEMS [2], fuel cell technology [3], micro-reactors [4], medical and biomedical devices [5] has motivated many researchers to investigate microscale transport phenomena. Microchannels have specific characteristics such as high surface area per unit volume and high heat transfer coefficient [2]. Moreover, microchannels are essential components of many microfluidic devices and new compact thermal solutions [1]. In addition, porous materials can be modeled as networks of microscale conduits; thus, transport properties of porous structures are closely related to the geometry of the considered microchannels [6,7]. Recently, microchannels with different cross-sectional geometries were fabricated for both commercial and scientific purposes. Therefore, investigation of fluid flow in channels with different cross-sections is important. Experimental studies conducted by Pfahler et al. [8,9], Harley et al. [10], Choi et al. [11], Stanley [12], and Gao et al. [13,14] confirmed that the continuum theory holds in micron size channels. Comprehensive reviews presented by Steinke and Kandlikar [15] and Papautsky et al. [16] discussed this subject; thus, existing solutions for large scale ducts are also applicable to microchannels.

Several analytical solutions for flow in non-circular channels are available in literature. Dryden et al. [17] based on the

analogy between fully-developed velocity profile and stress function in elasticity, reported velocity distribution in rectangular channels. Purday's model [18] presented a simple approximation for velocity distribution and Truskey et al. [19] employed separation of variable technique and developed exact velocity distribution in rectangular ducts. Solutions of flow in equilateral and isosceles triangular conduits are presented by Dryden et al. [17] and Sparrow [20], respectively. An isosceles trapezoid is an important shape since this cross-section is formed as a result of etching process in silicon wafers [21]. Shah [22] employing a discrete least method, obtained solutions for fully-developed flow in a variety of geometries including: trapezoidal, triangular with and without round corners, and rhombic cross-sections. Leveque solution for flow in an elliptical duct is reported by Richardson [23]. Cheng [24] employed 9 point matching method to determine the velocity profile and Poiseuille number for  $m$ -sided regular polygonal ducts. Fully developed flow in ducts with several irregular cross-sections are also solved, see for example [25-28]. A comprehensive review of the pertinent literature is available in Shah and London [29].

The major drawback in using microsystems is their high pressure drop, resulted from their small cross-sectional length scale [30]. Bahrami et al. [31,32] developed a general model for predicting pressure drop in microchannels of arbitrary cross-section. Using the analytical solution for elliptical duct and the concept of Saint-Venant principal in torsion, they showed that the Poiseuille number,  $f Re$ , where  $f$  is the Fanning friction factor and  $Re$  is the Reynolds number, is a function of the polar moment of inertia, area and perimeter of the cross-section of the channel. Their model showed good agreement with experimental and numerical data for a wide variety of cross-sections such as: rectangular, trapezoidal, triangular, circular, and moon-shaped. However, they did not provide the velocity distribution in the abovementioned microchannels.

An in-depth knowledge of velocity distribution plays a key role in determining other transport properties of microchannels such as heat and mass transfer coefficients. However, the authors were not able to find any general solutions for fully-developed flow in ducts. As such, having a generalized solution for the velocity distribution in microchannels is a great value; this is the subject of the present work.

Regular polygon and hyperellipse are flexible geometries that can cover a wide range of simply connected shapes, such as square, triangle, hexagon, rectangle, ellipse, rhomboid, and star-shaped. Therefore, the solution of flow through polygonal and hyperelliptical channels will be valid for a wide range of common geometries; thus, can be considered as a general solution.

In this study, an analytical solution is developed to predict the velocity distribution and the pressure drop of fully-developed laminar flow in both hyperelliptical and polygonal mini/microchannels. The proposed solution is validated through comparison with existing theoretical models and experimental data collected from different sources for a variety of geometries, including: circular, rectangular, elliptical, triangular and rhombic cross-sections.

## 2 CONSIDERED GEOMETRIES

### 2.1 HYPERELLIPSE

In the first quadrant, a hyperellipse is described by:

$$r_0 = \frac{a}{((\cos \theta)^n + (\sin \theta / \varepsilon)^n)^{1/n}}, \quad 0 < \varepsilon = \frac{b}{a} \leq 1 \quad (1)$$

where  $\varepsilon$  is the aspect ratio,  $a$  and  $b$  are the major and minor axes of the cross-section, respectively. As shown in Figs. 1 and 2, by varying parameter  $n$ , one can create several geometries. For  $n < 1$  the resulting geometry is a cross-section with convex sides, i.e., star-shaped geometry. Equation (1) with  $n = 1$  results in a rhomboid and when  $n = 2$  yields an ellipse; for  $a = b$ , the consequent geometry is a circle. For  $n > 2$ , a rectangle with round corners is created and when  $n \rightarrow \infty$  the resulting geometry becomes a rectangle; in the special case of  $a = b$  it represents a square and for  $a \ll b$  it yields parallel plates. Due to manufacturing processes, some of the flow passages have round corners. The hyperellipse geometry also covers these cross-sections. The cross-sectional area of a hyperellipse can be calculated from [33]:

$$A = 4a^2\varepsilon \frac{\sqrt{\pi} \Gamma\left(\frac{n+1}{n}\right)}{4^{1/n} \Gamma\left(\frac{n+2}{2n}\right)} \quad (2)$$

where  $\Gamma(\cdot)$  is the gamma function. The perimeter of the hyperellipse does not have a closed form solution and must be calculated from the following integral:

$$\Gamma_c = 4 \int_0^{\pi/2} \sqrt{\left(\frac{dr_0}{d\theta}\right)^2 + r_0^2} d\theta \quad (3)$$

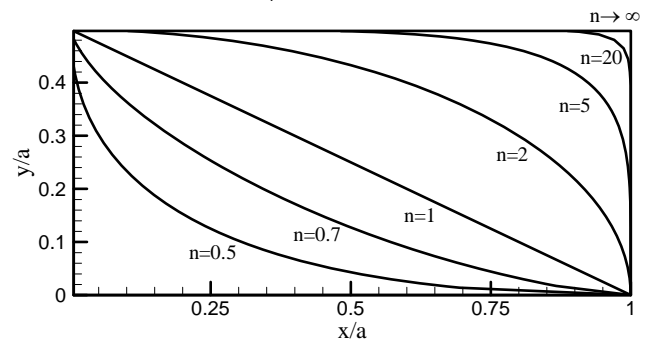


Figure 1: Effect of  $n$  on the shape of the hyperellipse equation in the first quadrant,  $\varepsilon = 0.5$ .

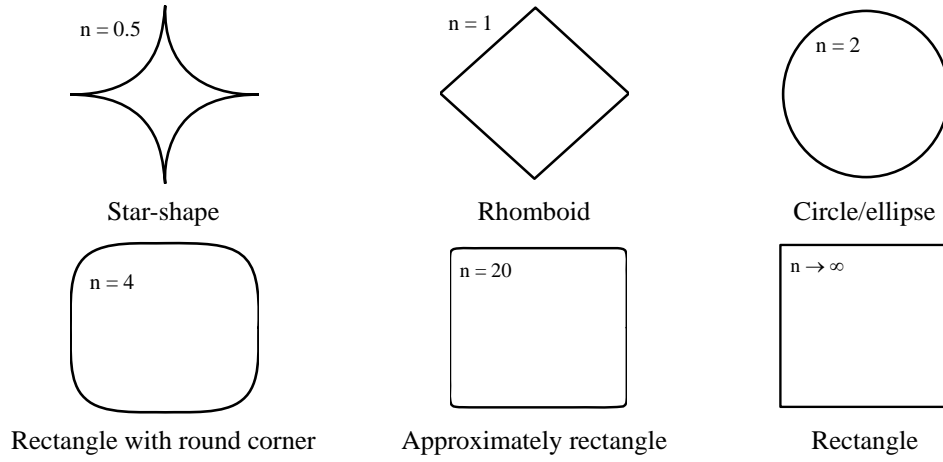


Figure 2: Different geometries covered by hyperellipse geometry.

## 2.1 REGULAR POLYGON

As shown in Fig. 3, the  $m$ -sided regular polygon ducts covers a wide range of geometries. For  $m = 3$ , the consequent geometry is an equilateral triangle; when  $m = 4$  and  $6$  the shapes become a square and a hexagon, respectively. A circle is a polygon with infinite number of sides, i.e.,  $m \rightarrow \infty$ . The cross-sectional area of the polygonal channels is:

$$A = \frac{m s^2}{\tan \frac{\pi}{m}} \quad (4)$$

and its perimeter is calculated as:

$$\Gamma_c = 2 m s \quad (5)$$

As shown in Fig. (3), all of the hatched regions surrounded by symmetry lines are triangles with different vertex angles.

## 3 PROBLEM FORMULATION

Fully-developed, laminar, constant properties, and incompressible flow in microchannels with constant hyperelliptical and polygonal cross-sections is considered. The compressibility effects can be neglected for the Mach numbers lower than 0.3 [34]; thus, the present analysis is acceptable for all Newtonian liquids and gas flows with  $Ma < 0.3$ . Using the

abovementioned assumptions, the momentum equation reduces to Poisson's equation [34]:

$$\frac{dP}{dz} = \mu \left( \frac{\partial^2 u}{\partial r^2} + \frac{1}{r} \frac{\partial u}{\partial r} + \frac{1}{r^2} \frac{\partial^2 u}{\partial \theta^2} \right) \quad (6)$$

where  $\mu$  is the fluid viscosity. Using the geometrical symmetry, only a portion of the cross-section is considered in the analysis, as shown in Figs. 4 and 5. Applicable boundary conditions for hyperelliptical channels are:

$$\left. \frac{\partial u}{\partial \theta} \right|_{\theta=\frac{\pi}{2}} = 0, \quad \left. \frac{\partial u}{\partial \theta} \right|_{\theta=0} = 0, \quad u(r_0) = 0 \quad (7)$$

The first two equations are obtained from the existing symmetry in the hyperellipse geometry. Moreover, the velocity should be bounded. The general solution of the Poisson's equation, Eq. (3), in the cylindrical coordinate is [35]:

$$u = A_1 + B \ln r + \frac{r^2}{4\mu} \left( \frac{dP}{dz} \right) + \sum_{k=1}^{\infty} (C_k r^k + D_k r^{-k}) (E_k \cos k\theta + F_k \sin k\theta) \quad (8)$$

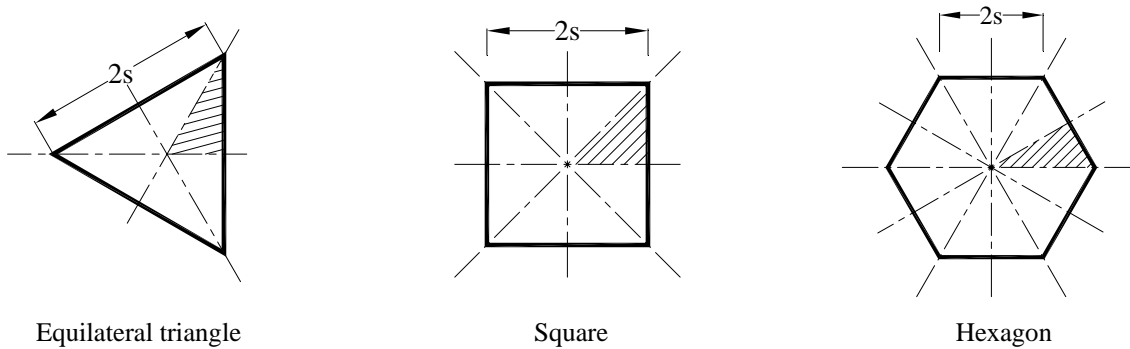


Figure 3: Polygons with different number of sides,  $m$ .

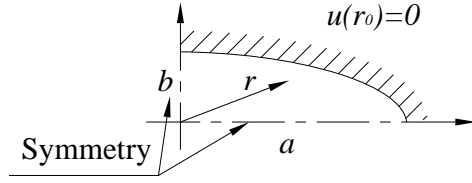


Figure 4: Hyperelliptical cross-section and applicable boundary conditions.

The unknown coefficients  $A_1$ ,  $B$ ,  $C_k$ ,  $D_k$ ,  $E_k$ , and  $F_k$  should be calculated through applying the boundary conditions, Eq. (4). At  $r = 0$ , the velocity must have a finite value; thus,  $B = D_k = 0$ . Since  $(dP/dz)$  remains constant for fully-developed flows, Eq. (5) can be simplified as:

$$u = \frac{1}{\mu} \left( \frac{dP}{dz} \right) \left[ A_1 + \frac{r^2}{4} + \sum_{k=1}^{\infty} (r^k) (E_k \cos k\theta + F_k \sin k\theta) \right] \quad (9)$$

where  $A_1$ ,  $E_k$ , and  $F_k$  are still unknown constants. The symmetry conditions at  $\theta = 0$  and  $\theta = \pi/2$  result in  $F_k = 0$  and  $k = 2, 4, 6, \dots$ , respectively. After non-dimensionalizing, Eq. (9) reduces to:

$$u^* = \left[ 1 - \frac{1}{4A_1} \eta^2 + \sum_{i=1}^{\infty} \frac{C_i}{A_1} \eta^{2i} \cos 2i\theta \right], \quad (10)$$

$$u^* = \frac{u}{U_{max}} = \frac{u}{\frac{1}{\mu} \left( \frac{dP}{dz} \right) A_1 a^2}, \quad \eta = \frac{r}{a}$$

The last boundary condition, i.e., the no-slip condition,  $u^*(\eta_0) = 0$ , on the channel wall should be used to calculate the rest of unknown coefficients in Eq. (10). Substituting for  $\eta_0$  from Eq. (1), one can write:

$$\left[ A_1 - \frac{1}{4} \frac{1}{((\cos \theta)^n + (\sin \theta / \varepsilon)^n)^{2/n}} + \sum_{i=1}^{\infty} C_i \frac{\cos 2i\theta}{((\cos \theta)^n + (\sin \theta / \varepsilon)^n)^{2i/n}} \right] = 0 \quad (11)$$

This equation is a function of  $\theta$ . To evaluate the coefficients, following [36], we truncate the series from the  $m$ th term and apply Eq. (11) over  $m+1$  different  $\theta$ s and solve the resulting set of linear equations.

The same approach can be followed for polygonal ducts, shown in Fig. 5. The difference between the two geometries is the location of the symmetry lines. Applicable symmetry boundary conditions for polygonal cross-section are:

$$\left. \frac{\partial u}{\partial \theta} \right|_{\theta=\frac{\pi}{m}} = 0, \quad \left. \frac{\partial u}{\partial \theta} \right|_{\theta=0} = 0 \quad (12)$$

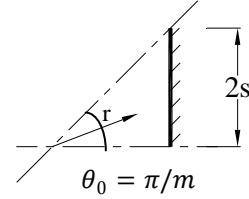


Figure 4: Considered geometry for modeling polygonal cross-section.

where  $m$  is the number of sides. Using Eq. (12), the dimensionless velocity distribution becomes:

$$u^* = \left[ 1 - \frac{1}{4A_1} \eta^2 + \sum_{i=1}^{\infty} \frac{C_i}{A_1} \eta^{2mi} \cos 2mi\theta \right], \quad (13)$$

$$u^* = \frac{u}{U_{max}} = \frac{u \left( \tan \frac{\pi}{m} \right)^2}{\frac{1}{\mu} \left( \frac{dP}{dz} \right) A_1 s^2}, \quad \eta = \frac{r \tan \frac{\pi}{m}}{s}$$

Applying no-slip boundary condition, the unknown coefficients can be determined. The calculated coefficients for several hyperelliptical and polygonal ducts are listed in Tables 1 and 2, respectively.

Note that we apply the no-slip boundary condition on a few points over the wall to find the same number of coefficients; this approach is an approximation. Therefore, one should be aware that Eq. (11) may not hold over the whole boundary. Thus, the minimum number of terms that should be included in the analysis without loss of accuracy is important. In addition, it is noteworthy that Eq. (11) is in cylindrical coordinate system. As such, for cross-sections that significantly deviate from elliptical shape, more terms of the series solution should be included in the analysis.

To verify the present approach, in Figs. 6-8 the predicted non-dimensional velocity distributions for elliptical and rectangular cross-sections are compared with the analytical solutions of Richardson [23] and Truskey et al. [19], respectively. The hyperellipse equation, Eq. (1), for  $n \rightarrow \infty$  yields a rectangle; however,  $n = 20$  is large enough to produce comparable results, see Fig. 1. Figures 6-8 show that the predicted contours of constant non-dimensional velocities are in full agreement with the analytical results for both elliptical and rectangular cross-sections. The solution for a polygonal duct with 3 sides, i.e., equilateral triangular, is successfully compared with the solution of Dryden et al. [17] in Fig. 9.

The maximum velocities in the channel are also compared with analytical results for the considered geometries in Table 3. Tabulated results justify the accuracy of the developed solution.

Table 1: Coefficients in Eq. (10) for hyperelliptical ducts.

<i>n</i> = 20, rectangle							
	$\varepsilon = 0.2$	$\varepsilon = 0.25$	$\varepsilon = 0.4$	$\varepsilon = 0.5$	$\varepsilon = 0.6$	$\varepsilon = 0.8$	$\varepsilon = 1$
$A_1$	0.020	0.031	0.077	0.114	0.153	0.229	0.296
$C_1$	0.249	0.248	0.225	0.195	0.158	0.076	0.000
$C_2$	-0.002	-0.011	-0.032	-0.045	-0.051	-0.052	-0.046
$C_3$	-0.009	-0.003	-0.018	-0.013	-0.014	-0.004	0.000
$C_4$	0.001	-0.014	-0.002	0.000	0.004	0.000	0.000
$C_5$	-0.009	0.000	0.000	0.000	0.000	0.000	0.000
<i>n</i> = 4, rectangle with round corner							
	$\varepsilon = 0.2$	$\varepsilon = 0.25$	$\varepsilon = 0.4$	$\varepsilon = 0.5$	$\varepsilon = 0.6$	$\varepsilon = 0.8$	$\varepsilon = 1$
$A_1$	0.020	0.031	0.075	0.111	0.149	0.223	0.285
$C_1$	0.248	0.244	0.216	0.184	0.149	0.071	0.000
$C_2$	-0.011	-0.017	-0.036	-0.044	-0.045	-0.042	-0.035
$C_3$	0.000	-0.007	-0.002	-0.002	0.000	0.000	0.000
$C_4$	-0.007	0.000	-0.004	0.000	-0.003	-0.002	0.000
<i>n</i> = 2, ellipse							
	$\varepsilon = 0.2$	$\varepsilon = 0.25$	$\varepsilon = 0.4$	$\varepsilon = 0.5$	$\varepsilon = 0.6$	$\varepsilon = 0.8$	$\varepsilon = 1$
$A_1$	0.019	0.029	0.069	0.100	0.132	0.195	0.250
$C_1$	0.231	0.221	0.181	0.150	0.118	0.055	0.000
<i>n</i> = 1, rhomboid							
	$\varepsilon = 0.2$	$\varepsilon = 0.25$	$\varepsilon = 0.4$	$\varepsilon = 0.5$	$\varepsilon = 0.6$	$\varepsilon = 0.8$	$\varepsilon = 1$
$A_1$	0.016	0.023	0.048	0.065	0.084	0.117	0.149
$C_1$	0.164	0.143	0.096	0.075	0.054	0.027	0.000
$C_2$	0.310	0.312	0.237	0.202	0.175	0.131	0.101
$C_3$	-0.820	-0.715	-0.251	-0.186	-0.063	-0.025	0.000
$C_4$	1.377	1.106	0.119	0.094	0.000	0.000	0.000
$C_5$	-1.253	-0.961	0.000	0.000	0.000	0.000	0.000
$C_6$	0.457	0.341	0.000	0.000	0.000	0.000	0.000
$\varepsilon = 1$ , star-shape							
	<i>n</i> = 0.9	<i>n</i> = 0.8	<i>n</i> = 0.7	<i>n</i> = 0.6			
$A_1$	0.129	0.107	0.085	0.062			
$C_1$	0.000	0.000	0.000	0.000			
$C_2$	0.121	0.149	0.205	0.304			
$C_3$	0.000	0.000	0.000	0.001			
$C_4$	0.000	-0.006	-0.039	-0.176			
$C_5$	0.000	0.000	0.000	-0.001			
$C_6$	0.000	0.000	0.000	0.060			

$$u^* = \left[ 1 - \frac{1}{4A_1} \eta^2 + \sum_{i=1}^{\infty} \frac{C_i}{A_1} \eta^{2i} \cos 2i\theta \right]$$

Table 2: Coefficients in Eq. (13) for polygonal ducts.

	$m = 3$	$m = 4$	$m = 5$	$m = 6$	$m = 7$	$m = 8$	$m = 12$	$m \rightarrow \infty$
$A_1$	0.333	0.296	0.278	0.270	0.265	0.261	0.255	0.250
$C_1$	-0.083	-0.046	-0.021	-0.021	-0.015	-0.012	-0.006	0.000

$$u^* = \left[ 1 - \frac{1}{4 A_1} \eta^2 + \frac{C_1}{A_1} \eta^{2m} \cos(2m\theta) \right]$$

$$A_1 = 0.247 + \frac{0.767}{m^2}, \quad C_1 = \frac{1}{6.01 - 3.12 m - 0.965 m^2}$$

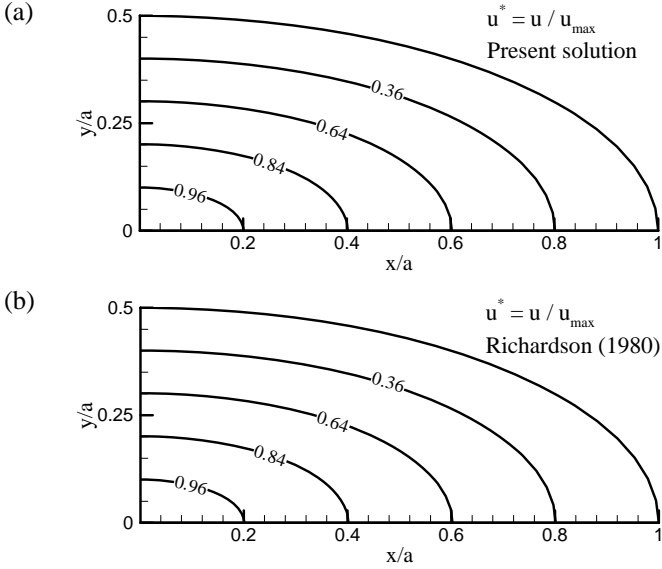


Figure 6: Contours of constant velocity for elliptical channel with  $\varepsilon = 0.5$ , a) present model, b) Richardson et al. [23].

#### 4 PRESSURE DROP AND POISEUILLE NUMBER

Pressure drop is an important characteristic of any system that should be considered in the design procedure. Once the coefficients are known, one can integrate Eqs. (7) and (13) to find the pressure drop for a specific volumetric flow rate,  $Q$ , for hyperelliptical and polygonal ducts, respectively:

$$\left( \frac{dP}{dz} \right)_{Hyperellipse} = \frac{\mu Q}{a^2} \left\{ \iint \left[ A_1 - \frac{1}{4} \eta^2 + \sum_{i=1}^{\infty} C_i \zeta^{2i} \cos 2i\theta \right] dA \right\}^{-1} \quad (14)$$

$$\left( \frac{dP}{dz} \right)_{Polygon} = \frac{\mu Q \left( \tan \frac{\pi}{m} \right)^2}{s^2} \left\{ \iint \left[ A_1 - \frac{1}{4} \eta^2 + \sum_{i=1}^{\infty} C_i \eta^{2mi} \cos 2mi\theta \right] dA \right\}^{-1} \quad (15)$$

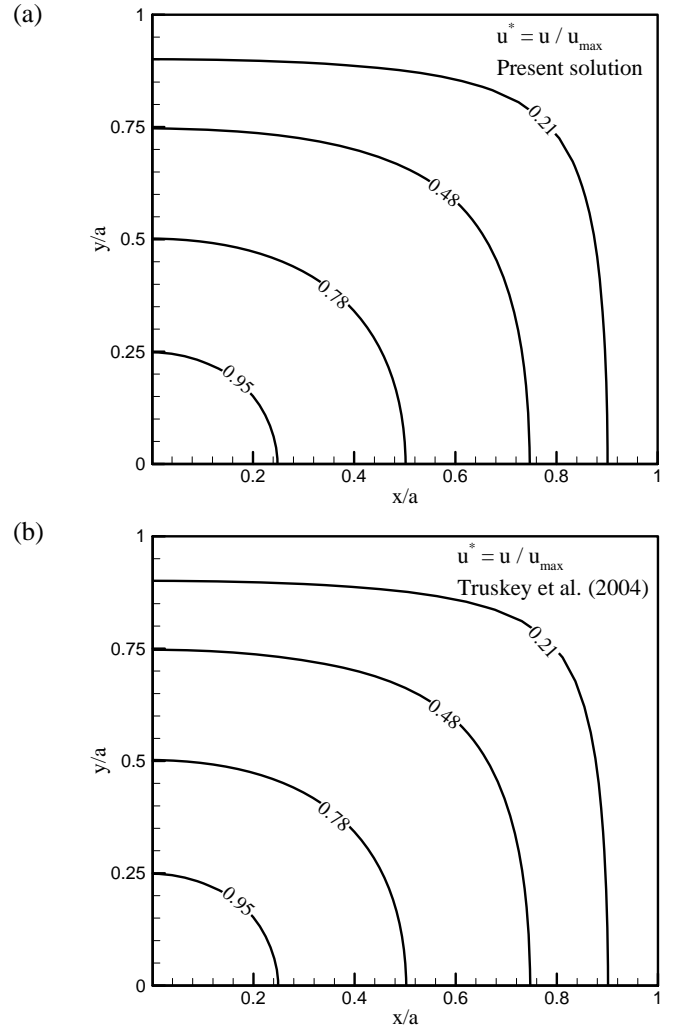


Figure 7: Contours of constant velocity for squared channel, a) present model, b) Truskey et al. [19].

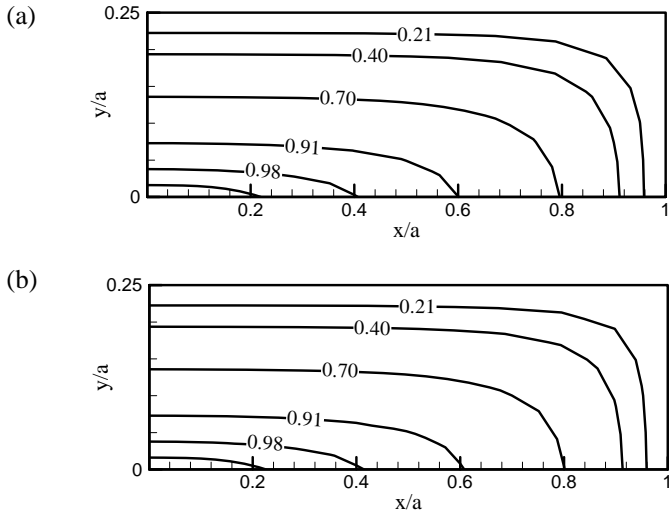


Figure 8: Contours of constant velocity for rectangular channel with  $\varepsilon = 0.25$ , a) present model, b) Truskey et al. [19].

It can be seen that the pressure drop is a function of the volumetric flow rate and dimensions of the cross-section. Poiseuille number,  $fRe$ , is the common dimensionless number used for analysing pressure drop in channels. The value of  $fRe$  depends on the characteristic length scale used for defining the Reynolds number. Selection of the characteristic length is an arbitrary choice and should not affect the final solution, i.e., the pressure drop. However, a more appropriate length scale leads to more consistent results, especially when various cross-sections are considered. A circular duct is fully described with its diameter, thus the obvious length scale is the diameter (or radius). For non-circular cross-sections, the selection is not as clear; many textbooks and researchers have conventionally chosen the hydraulic diameter [34]. Figure 10a and b shows the comparison of the analytical solutions of  $fRe$ , for elliptical, rectangular, and rhomboid cross-sections based on the hydraulic diameter and the square root of area, respectively. It can be observed that using the square root of area as the characteristic length leads to similar trends in analytical solutions of  $fRe$  for the considered geometries. The values of  $fRe_{\sqrt{A}}$  can be determined from the following equation:

$$fRe_{\sqrt{A}} = \frac{2 A^{5/2} dP}{\mu Q \Gamma_c dz} \quad (11)$$

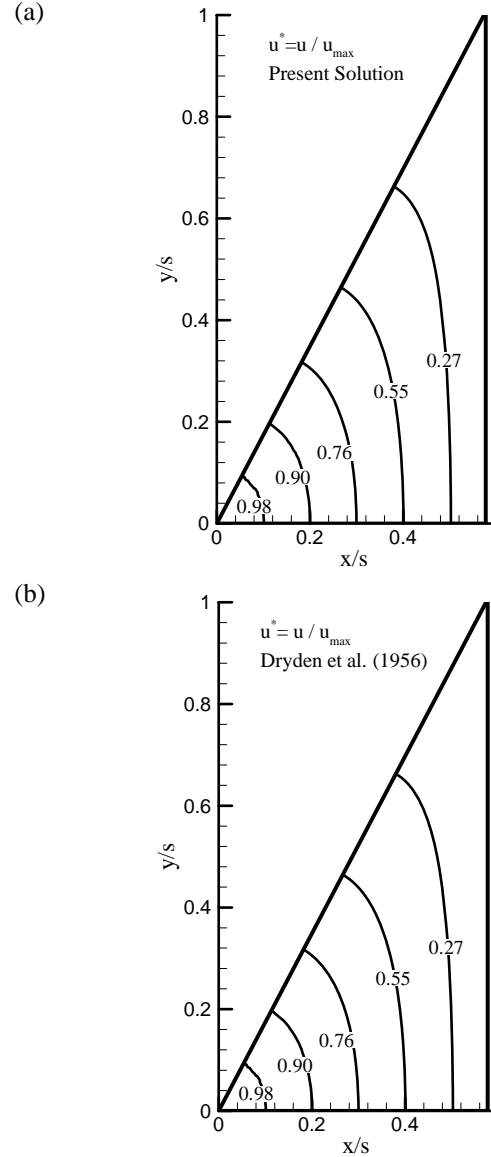


Figure 9: Contours of constant velocity for a sector of triangular channel, a) present model, b) Dryden et al. [17].

Table 3: Comparison of the maximum velocities for elliptical and rectangular channels with other analytical solutions.

	Elliptical cross-section Richardson [23]	$n = 2$ Present solution	Rectangular cross-section Truskey et al. [19]	$n = 20$ Present solution
$\varepsilon = 1$	0.2500	0.2500	0.2947	0.2946
$\varepsilon = 0.5$	0.1000	0.1000	0.1139	0.1138
$\varepsilon = 0.33$	0.0500	0.0500	0.0545	0.0545
$\varepsilon = 0.25$	0.0294	0.0294	0.0311	0.0311
$\varepsilon = 0.2$	0.0192	0.0192	0.0200	0.0200

where  $\Gamma_c$  is the cross-section perimeter and  $dP/dz$  is calculated from Eqn. (14) and (15). Values of  $f Re_{\sqrt{A}}$  obtained from the present model and the correlations proposed by Shah and London [29] are plotted versus the cross-sectional aspect ratio for rectangular, elliptical and rhombic ducts in Fig. 11. The results have an excellent agreement. The rectangular microchannels have the highest  $f Re_{\sqrt{A}}$  in comparison to other considered geometries with the same cross-sectional area. In addition, it can be seen that the Poiseuille number has a reverse relationship with aspect ratio.

In Fig. 12,  $f Re_{\sqrt{A}}$  values for polygonal channels calculated using the present solution are compared with the results of Shah and London [29] and the results are in complete agreement. More importantly, the minimum value of  $f Re_{\sqrt{A}}$  occurs for  $m = 6$ ; this means that hexagonal ducts have the minimum pressure drop in comparison with other polygonal shapes.

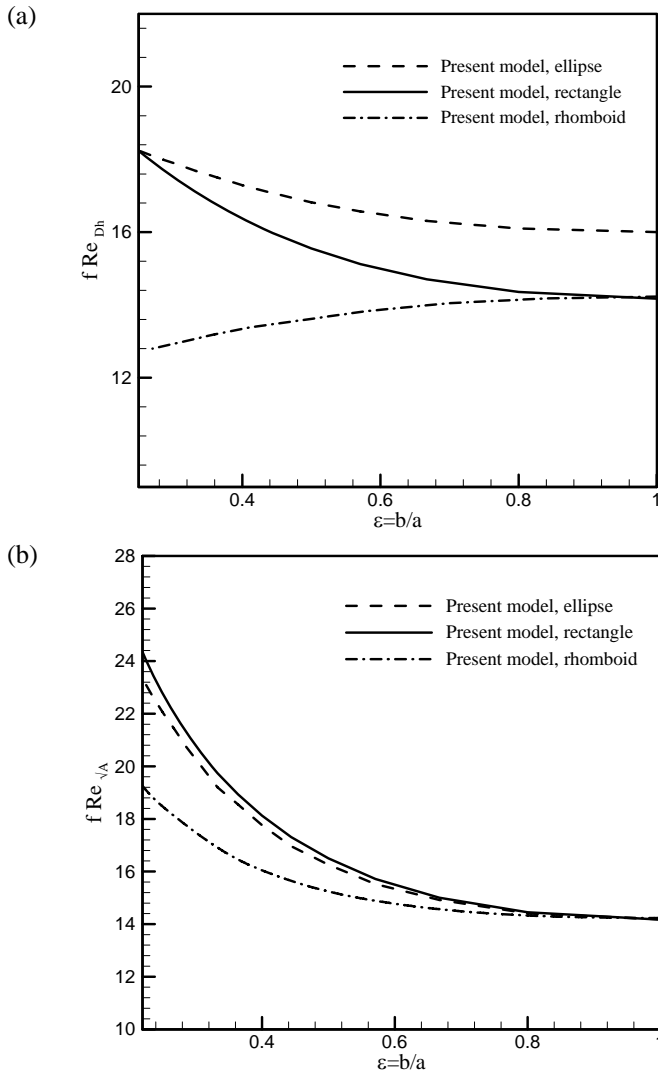


Figure 10:  $f Re$  for different geometries using (a) hydraulic diameter and (b) square root of area as characteristic length.

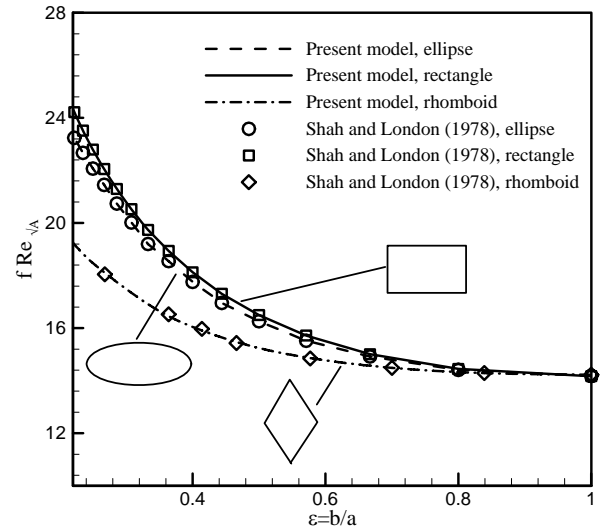


Figure 11: Values of  $f Re_{\sqrt{A}}$  obtained from present model and existing correlations [29] for different values of  $n$ , hyperelliptical ducts.

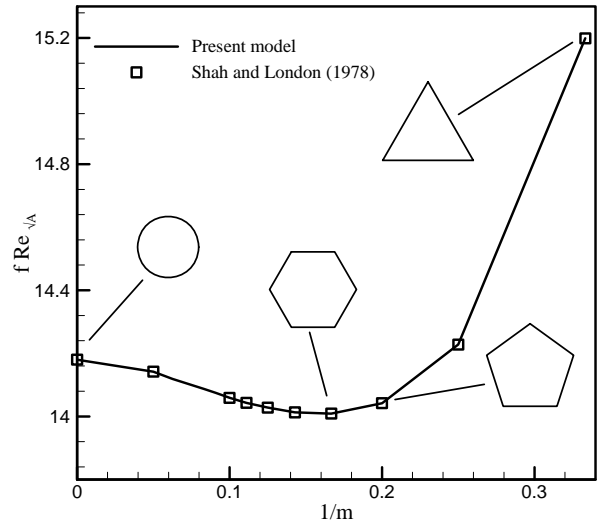


Figure 12: Values of  $f Re_{\sqrt{A}}$  obtained from present model and existing correlations [29] for different values of  $m$ , polygonal ducts.

To determine the Poiseuille number,  $f Re$ , Bahrami et al. [30, 31] started from the analytical solution of elliptical channel. They also selected  $\sqrt{A}$  as the length scale in their study. The final result was presented in an easy-to-use form, as a function of cross-sectional area and polar moment of inertia. In Table 4 the non-dimensional values of the pressure drop for elliptical ducts are compared with the analytical model of Richardson [23] and the model of Bahrami et al. [31]. All solutions capture the same results for elliptical channels. The values of the pressure drop obtained from the present solution for rectangular cross-section and the approximate model of

Bahrami et al. [31] are listed in Table 5. It can be seen that the difference between the proposed model and Bahrami et al.'s model [31] is less than 8%. Therefore, it is an accurate alternative approach for prediction of approximate values of pressure drop.

Table 4:  $f Re_{\sqrt{A}}$  for elliptical ducts obtained from different models.

$\varepsilon$	$f Re_{\sqrt{A}}$ Richardson [23]	$f Re_{\sqrt{A}}$ Present solution	$f Re_{\sqrt{A}}$ Bahrami et al. [31]
1	14.18	14.18	14.18
0.5	16.26	16.26	16.26
0.33	19.20	19.20	19.20
0.25	22.07	22.07	22.07
0.2	24.65	24.65	24.65

Table 5:  $f Re_{\sqrt{A}}$  for rectangular ducts obtained from different models.

$\varepsilon$	$f Re_{\sqrt{A}}$ Present solution	$f Re_{\sqrt{A}}$ Bahrami et al. [31]
1	14.17	13.16
0.5	16.50	15.51
0.33	19.74	18.99
0.25	22.79	22.37
0.2	25.60	25.50

#### 4.1 COMPARISON WITH EXPERIMENTAL DATA

Several researchers have reported experimental data for pressure drop in rectangular microchannels. Stanly [12] studied flow of water, nitrogen, and helium in arrays of rectangular microchannels. The channels were fabricated by machining aluminum substrates and then covering them with glass plates. Papautsky et al. [37] fabricated arrays of pipettes with width varying from  $150 \mu m$  to  $600 \mu m$ . Their data for low aspect ratios consistently were 20% larger than theoretical values. Therefore, only their results for aspect ratios larger than 0.05 are included here.

Liu and Garimella [38] carried out experiments and measured the friction factor in rectangular microchannels. They did not observe any scale-related phenomena in their experiments and concluded that the conventional theory can be used to predict the flow behaviour in microchannels in the range of dimensions considered.

Wu and Cheng [39] conducted experiments and measured the friction factor of laminar flow of deionized water in smooth silicon microchannels of trapezoidal, rectangular, and triangular cross-sections.

Jung and Kwak [40] experimentally measured fluid flow and heat transfer in rectangular silicon microchannels with different aspect ratios. But, they only reported the friction factor for two geometries,  $\varepsilon = 0.5$  and 1.

Recently, Akbari et al. [41] performed experiments to measure pressure drop in rectangular microchannels, fabricated in Polydimethylsiloxane (PDMS). The fabricated channels were cut in different locations to make sure that they have a rectangular cross-section. They tested several samples with a wide range of cross-sectional aspect ratios.

In Fig. 9 the values of Poiseuille number are plotted against experimental data collected from the abovementioned sources. It can be seen that the present solution captures the trends of experimental data of liquid flow in rectangular ducts fabricated using different materials over a wide range of aspect ratios. Moreover, it can be seen that the model of Bahrami et al. [31] provides good approximations for Poiseuille number.

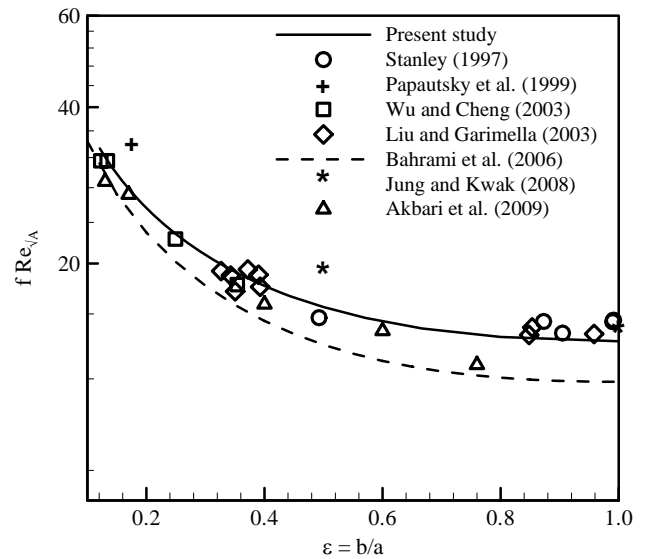


Figure 9: Comparison of  $f Re_{\sqrt{A}}$  values for rectangular channels with experimental data.

## 5 CONCLUSIONS

Analytical solutions are proposed for the laminar, fully-developed flow through hyperelliptical and polygonal mini/microchannels. The present method enables one to predict velocity distribution and pressure drop for several common fabricated geometries for industrial applications including: circular, elliptical, rectangular, rhomboid, triangular, and hexagonal ducts. The approach is based on using the general solution Poisson's equation in the form of trigonometric series expansion. Therefore, the required

coefficients are reported for a wide range of geometries. Using the developed solution for velocity distribution, pressure drops and Poiseuille numbers are determined for a variety of cross-sections. The predicted values are verified through comparison with analytical solutions for elliptical, circular, rectangular, rhombic, and polygonal ducts. Predicted results are also successfully compared with experimental data collected by others for rectangular channels.

## 6 ACKNOWLEDGMENTS

The authors gratefully acknowledge the financial support of the Natural Sciences and Engineering Research Council of Canada, (NSERC).

## 7 REFERENCES

- [1] D.B. Tuckerman, R.F. Pease, 1981, "High-Performance Heat Sinking for VLSI," IEEE Electron Device Letters, Vol. **5**, pp. 126–129.
- [2] C.M. Ho, Y.C. Tai, 1998, "Micro-Electro-Mechanical-Systems (MEMS) and Fluid Flows," Annual Review of Fluid Mechanics, Vol. **30**: 579-612.
- [3] S.W. Cha, R. O'Hayre, F.B. Prinz, 2004, "The Influence of Size Scale on the Performance of Fuel Cells," Solid State Ionics, Vol. **175**, pp. 789–795.
- [4] A.I. Günther, S.A. Khan, M. Thalmann, F. Trachsel, K.F. Jensen, 2004, "Transport and reaction in microscale segmented gas–liquid flow," Lab on a Chip, Vol. **4**, pp. 278–286.
- [5] C. Efenhauser, A. Manz, M. Widmor, 1993, "Glass chips for high-speed capillary electrophoresis separation with submicrometer plate heights, Analytical Chemistry, Vol. **65**, pp. 2637-2642.
- [6] M. Kaviany, 1992, "Principles of Heat Transfer in Porous Media," Springer-Verlag, New York.
- [7] A. Tamayol, M. Bahrami, 2009, "Analytical Determination of Viscous Permeability of Fibrous Porous Media," International Journal of Heat Mass Transfer, Vol. **52**, pp. 3691-3701.
- [8] J. Pfahler, J. Harley, H. Bau, and J.N. Zemel, 1991, "Liquid Transport in Micron and Submicron Channels," Sensors and Actuators, Vol. **A21–A23**, pp. 431–437.
- [9] Pfahler, J., Harley, J., Bau, H., and Zemel, J.N., 1991, "Gas and Liquid Transport in Small Channels," ASME Micromechanical. Sensors Actuators Systems, Vol. **32**, 49-58.
- [10] J.C. Harley, Y. Huang, H. Bau, J.N. Zemel, 1995, "Gas Flow in Microchannels," J. Fluid Mech. 284:257–74
- [11] S.B. Choi, R.F. Barron, R.O. Warrington, 1991, "Fluid Flow and Heat Transfer in Microtubes," ASME Micromechanical Sensors, Actuators, and Systems, Vol. **32**, pp. 123-134.
- [12] R.S. Stanley, 1997, "Two-phase flow in microchannels," Ph.D. Thesis, Louisiana Tech. University.
- [13] P. Gao, S.L. Person, M.F. Marinnet, 2002, "Scale Effects on Hydrodynamics and Heat Transfer in Two-Dimensional Mini and Microchannels," International Journal of Thermal Sci., Vol. **41**, pp. 1017–1027.
- [14] B. Cao, G.W. Chen, Q. Yuan, 2005, "Fully Developed Laminar Flow and Heat Transfer in Smooth Trapezoidal Microchannel," International Communications Heat and Mass Transfer, Vol. **32**, pp. 1211-1220.
- [15] M.E. Steinke and S.G. Kandlikar, 2006, "Single-phase liquid friction factors in microchannels," International Journal of Thermal Sciences, Vol. **45**, pp. 1073-1083.
- [16] I. Papautsky, T. Ameel, and A.B. Frazier, 2001 "A Review of Laminar Single Phase Flow in Microchannels," ASME International Mechanical Engineering Conference and Exposition, Nov. 21-26 2001, New York, USA.
- [17] H.L. Dryden, F.D. Murnaghan, and H. Bateman, 1932, "Hydrodynamics," Bulletin of The National Natural Resources, Vol. **84**, pp. 197-201.
- [18] H.F.P. Purday, 1949, "An Introduction to the Mechanics of Viscous Flow; Film Lubrication, the Flow of Heat by Conduction and Heat Transfer by Convection," Dover Publications.
- [19] G.A. Truskey, F. Yuan, D.E. Katz, 2004 "Transport Phenomena in Biological Systems," Pearson Prentice Hall, New Jerseys.
- [20] E.M. Sparrow, 1962, "Laminar Flow in Isosceles Triangular Ducts," AICHE Journal, Vol. **8**, pp. 599-604.
- [21] R. Sadasivam, R.M. Manglik, M.A. Jog, 1999, 'Fully-Developed Forced Convection through Trapezoidal and Hexagonal Ducts,' International Journal of Heat Mass Transfer, Vol. **42**, pp. 4321-4331.
- [22] R. K. Shah, 1975, "Laminar Flow Friction and Forced Convection in Duct of Arbitrary Geometry," International Journal of Heat Mass Transfer, Vol. **18**, pp. 849-862.
- [23] S.M. Richardson, 1980, "Leveque Solution for Flow in an Elliptical Duct," Letters Heat Mass Transfer, Vol. **7**, pp. 353-362.
- [24] K.C. Cheng, 1966, "Laminar Forced Convection in Regular Polygon Ducts with Uniform Peripheral Heat Flux," Proceeding of 3<sup>rd</sup> International Heat Transfer Conference, New York, pp. 64-76.
- [25] J. Ding, R.M. Manglik, 1996, "Analytical Solutions for Laminar Fully-Developed Flows in Double-Sine Shaped Ducts,' Heat and Mass Transfer, Vol. **31**, pp. 269-277.
- [26] L.Y. Ming, L.P. Chang, 2002, "Heat Transfer Coefficients of Laminar Flow in a Rhombic Duct with Constant Wall Temperature," Numerical Heat Transfer, Vol. **42**, pp. 285-296.
- [27] R.M. Manglik, A.E. Bergles, 1994, "Fully Developed Laminar Heat Transfer in Circular-Segment Ducts with

- Uniform Wall Temperature,” Numerical Heat Transfer, Vol. **26**, pp. 499-519.
- [28] D.H. Richardson, D.P. Sekulic, A. Campo, 2000, “Low Reynolds Number Flow Inside Microchannels with Irregular Cross-Sections,” Heat and Mass Transfer, Vol. **36**, pp. 187-193.
- [29] R.K. Shah, A.L. London, 1978, “Laminar Flow Forced Convection in Ducts,” Academic Press, New York.
- [30] M. Bahrami, A. Tamayol, P. Taheri, 2009, “Slip-Flow Pressure Drop in Microchannels of General Cross-Section,” ASME Journal of Fluid Engineering, Vol. **131**, pp. 1036-1044.
- [31] M. Bahrami, M.M. Yovanovich, J.R. Culham, 2006, “Pressure Drop of Laminar, Fully Developed Flow in Microchannels of Arbitrary Cross-Section,” ASME Journal of Fluid Eng., Vol. **128**, pp. 1036-1044.
- [32] M. Bahrami, M.M. Yovanovich, J.R. Culham, 2007, “A Novel Solution for Pressure Drop in Singly Connected Microchannels of Arbitrary Cross-Section,” International Journal of Heat and Mass Transfer, Vol. **50**, pp. 2492-2502.
- [33] M.M. Yovanovich, S.S. Burde, J.C. Thompson, 1976, “Thermal Constriction Resistance of Arbitrary Planar Contacts with Constant Flux,” AIAA 11th Thermophysics Conference San Diego, CA.
- [34] F.M White, 1984, “Viscous Fluid Flow,” McGraw-Hill, New York,.
- [35] S.J. Farlow, 1993, “Partial Differential Equations for Scientists and Engineers,” Dover Publication INC., NY.
- [36] E.M. Sparrow, A.L. Loeffler, 1959, “Longitudinal Laminar Flow between Cylinders Arranged in Regular Array,” AIChE, Vol. **5**, pp. 325-330.
- [37] I. Papautsky, B.K. Gale, S. Mohanty, T.A. Ameel, A.B. Frazier, 1999, “Effects of rectangular microchannel aspect ratio on laminar friction constant,” SPIE Conference on Microfluidic Devices and Systems II, Santa Clara, CA.
- [38] D. Liu, S. Garimella, 2004, “Investigation of Liquid Flow in Microchannels,” AIAA Journal of Thermophysical Heat Transfer, Vol. **18**, pp. 65–72.
- [39] H.Y. Wu, P. Cheng, 2003, “Friction Factors in Smooth Trapezoidal Silicon Microchannels with Different Aspect Ratios,” International Journal of Heat Mass Transfer, Vol. **46**, pp. 2519-2525.
- [40] J.Y. Jung, H.Y. Kwak, 2008, “Fluid flow and heat transfer in microchannels with rectangular cross-section,” Heat Mass Transfer, Vol. **44**, pp. 1041–1049.
- [41] M. Akbari, M. Bahrami, D. Sinton, 2009, Flow in Rectangular Microchannels: an Experimental Investigation, ASME Journal Fluid Eng., Vol. 131, pp. 041203-1-10.